water

MDPI

Article

Contamination Characteristics and Source Identification of Groundwater in Xishan Coal Mining Area of Taiyuan Based on Hydrochemistry and Sulfur–Oxygen Isotopes

Di Chen [1,2], Qiyan Feng [1,2,*] and Min Gong [1,2]

[1] Engineering Research Center of Ministry of Education for Mine Ecological Restoration, China University of Mining and Technology, NO.1 Daxue Street, Quanshan District, Xuzhou 221116, China
[2] School of Environment Science and Spatial Informatics, China University of Mining and Technology, NO.1 Daxue Street, Quanshan District, Xuzhou 221116, China
* Correspondence: fqycumt@126.com; Tel.: +86-13705205590; Fax: +86-051683591315

Abstract: Xishan mining area in Taiyuan is a typical coal industry cluster with a variety of coal-related industrial sites such as coal mines, power plants and coking plants, which seriously pollute the native ecological environment. Study of the hydrochemical characteristics and pollution sources of groundwater in the area can contribute to the ecological protection and remediation of regional groundwater resources. In this study, we collected surface water and groundwater samples from the Xishan mining area and measured and analyzed hydrochemical and sulfur–oxygen isotopes. Results showed that 64.7% of groundwater in the study area exceeded the sulfate standard due to the influence of the coal industry, with some karst groundwater up to 2000 mg/L. In the runoff and discharge area of karst groundwater, the proportion of anthropogenic input of SO_4^{2-} increased, which led to the hydrochemical type of karst groundwater gradually changing from HCO_3-Ca·Mg (recharge area) to SO_4-Ca·Mg (discharge area). Results of sulfur–oxygen isotope tests indicated that the $\delta^{34}S_{SO4}$ and $\delta^{18}O_{SO4}$ values of samples were −10.01~24.42‰ and −4.90~12.40‰, respectively, and the sulfur–oxygen isotope values of some karst groundwater were close to the dissolved end of sulfide minerals, indicating their sulfate mainly came from the oxidation of pyrite. Sulfate sources in groundwater water were parsed using IsoSource model. Calculated results revealed that sulfate in pore groundwater mostly originated from pyrite oxidation, and karst groundwater in the recharge area was mainly influenced by atmosphere precipitation, while groundwater in the runoff and discharge areas were significantly affected by pyrite oxidation, accounting for up to 90% in some karst groundwater. Comparing the sulfur–oxygen isotope values of karst groundwater in 1989, 2016 and 2022, we found that the $\delta^{34}S_{SO4}$ values in 2022 decreased significantly, which indicated the expansion of karst groundwater pollution in the Xishan mining area. This study highlights the pollution of regional groundwater by coal-related industrial agglomerations, and the groundwater pollution in the Xishan mining area requires urgent remediation and restoration.

Keywords: hydrochemical characteristics; sulfur–oxygen isotopes; source identification; Xishan mining area; water–rock interaction

Citation: Chen, D.; Feng, Q.; Gong, M. Contamination Characteristics and Source Identification of Groundwater in Xishan Coal Mining Area of Taiyuan Based on Hydrochemistry and Sulfur–Oxygen Isotopes. *Water* **2023**, *15*, 1169. https://doi.org/10.3390/w15061169

Academic Editors: Qiqing Wang and Shiliang Liu

Received: 15 February 2023
Revised: 12 March 2023
Accepted: 16 March 2023
Published: 17 March 2023

1. Introduction

Coal plays an important role in China's primary energy system [1]. During the process of coal resources development, a number of industrial zones have gradually formed in the main coal producing areas of Shanxi Province, mainly including coal mines, thermal power plants, coking plants, sorting plants and coal-washing plants. These coal-related plants cause different degrees of pollution of the surrounding environment during production and day-to-day activities. For example, coal gangue is produced during the process of coal mining, coal washing and coal separation, and thermal power plants produce large amounts of fly ash and desulfurization ash. These solid wastes usually accumulate directly

on the ground surface, and the leachate formed under the long-term drenching effect of atmospheric rainfall causes surface water pollution or direct infiltration to pollute groundwater [2]. Furthermore, as a large number of coal mines with backward capacity have been closed, the wastewater generated by these abandoned coal mines can also damage the ecological environment [3]. Coal-related industrial agglomerations are characterized by many types of industrial sites, a wide range of pollution and complex sources of pollutants, and the impact of such industrial agglomerations on the regional ecological environment needs more attention.

The hydrochemistry of surface and groundwater is influenced by rock weathering, the recharge and discharge process of runoff, occurrence conditions and human activities [4,5]. Based on hydrochemical parameters of different water bodies, the source and transformation law of surface-groundwater hydrochemical ions can be revealed by means of hydrochemical statistical diagrams [6]. Zhou et al., analyzed the main ion characteristics and controlling factors of surface water and groundwater in the upper reaches of Shule River by hydrochemical analysis [7]. Li et al., analyzed the hydrochemical characteristics of groundwater in karst wetland in different hydrological cycles by hydrochemical statistical diagrams and discussed the influence of natural and human factors on major chemical ions [8]. In addition to hydrochemical analysis, due to the exchange of matter and energy in the transformation of different water bodies, the source and circulation process of surface water and groundwater can be revealed by comprehensively analyzing the hydrochemistry and isotopic composition of water bodies [9,10]. Gu et al., analyzed the relationship between recharge and discharge of groundwater and surface water in the Liujiang Basin by environmental isotopes and hydrochemical analysis [11]. Liu et al., used hydrochemistry and stable isotopes of hydrogen and oxygen to reveal the temporal and spatial variation characteristics and recharge sources of surface water and groundwater in the Donggong River Basin [12].

Stable isotopes can be used to trace the source of water pollution. Sulfur isotopes of sulfate in nature have unique isotopic values associated with their sources [13], and there is little significant sulfur isotope fractionation during the biogeochemical cycle of sulfur, except for sulfate bacterial reduction [14]. Therefore, sulfur isotopes have become an important tool for tracing the source of sulfate in water [15]. SO_4^{2-} in acid mine drainage water is mainly derived from the oxidation of pyrite and thus has the same $\delta^{34}S_{SO4}$ value as pyrite [16], with $\delta^{18}O_{SO4}$ values depending mainly on the oxidation pathway of pyrite and the oxygen isotopic composition of its oxygen source [17]. Therefore, the analysis of the sulfur and oxygen isotope composition of sulfates ($\delta^{34}S_{SO4}$ and $\delta^{18}O_{SO4}$) can reveal the source of sulfate pollution and trace the pollution of underground water by acidic mine drainage [18]. For example, Li et al., used sulfur and oxygen isotopes to trace and quantify the pollution of acid mine drainage from Heshan Coal Mine and found that the groundwater in the mining area was basically affected by the infiltration of acid mine drainage, with the contribution ratio to groundwater sulfate ranging from 16% to 52% [16]. Zhao et al., analyzed the distribution characteristics of SO_4^{2-} and sulfur isotopes in karst groundwater in Niangziguan spring area, Shanxi Province. They have found that SO_4^{2-} in karst groundwater in northwest and southwest areas of the spring area was mainly from the dissolution of gypsum, while the high content of SO_4^{2-} and low $\delta^{34}S_{SO4}$ value of karst groundwater in the central confluence area of Spring mainly originated from coal mine water [19].

As a typical coal industry cluster, more than 200 coal mines, as well as coal-washing plants, sorting plants, thermal power plants, etc., are located in Xishan coal mining district. The mineable coal seams in the Xishan mining area contain medium- and high-sulfur coal, and the sulfide minerals associated with the coal seams and gangue are oxidized to form acid mine water [20]. The discharge of acid gangue leachate and mine water has caused serious pollution of the local environment. Especially in recent years, the acid mine water generated by some abandoned coal mines has further aggravated the pollution of regional surface and groundwater systems. In order to identify the pollution of regional

groundwater by typical coal-related industrial agglomerations, we collected surface water, mine water and gangue leachate groundwater from Xishan mining area to analyze the hydrochemical characteristics and pollution causes based on hydrochemical and sulfur–oxygen isotopes. This study can contribute to the elaboration of regional strategies for ecosystem restoration.

2. Hydrogeological Background of Study Area

Xishan coalfield is located in the eastern edge of Lvliang Mountain and the west side of Cenozoic fault basin in Taiyuan, with the geographical coordinates ranging from 111°50′55″ to 112°31′35″ E and 37°23′49″ to 38°02′14″ N. The northern part is a typical northern karst landform, and the mountains are mostly composed of hard carbonate rocks of the Cambrian and Ordovician age and Archean metamorphic rocks. The southeastern part is the Taiyuan fault basin, which is flat and generally high in the northwest and low in southeast [21]. Rivers of the study region belong to the Fen River system in the Yellow River Basin, and the main rivers are Fen River and its tributaries, such as Tunlan River, Yuanping River and Dachuan River. The main groundwater aquifers include the Middle Ordovician limestone karst aquifer, Taiyuan Formation fissure karst aquifer, Shanxi Formation and Xiashihezi Formation sandstone fissure aquifer and Quaternary gravel stratum pore aquifer. Groundwater Springs leak out along Fen River Valley and mountains. The rocks in the karst aquifer are mainly Cambrian and Ordovician carbonate rocks, and the groundwater flows from the north and northwest to south and southeast, forming karst springs. The fractured aquifers mainly include clastic rocks, clastic rocks intercalated with carbonate rocks, metamorphic rocks and magmatic rocks, mainly sandstone and limestone. The groundwater flows from northwest to southeast. The porous aquifers are composed of loose rocks, and the main recharge sources are atmospheric precipitation and surface water.

The study area is located in the Jinci Spring area, which is divided into the runoff recharge area, runoff discharge area and alluvial plain area according to hydrogeological units. Most of the areas north of Tunlan River and Fen River belong to the recharge–runoff area of karst groundwater, while the area south of Fen River belongs to the runoff–discharge area. Jinci Spring is the discharge point of karst groundwater [22]. The main recharge of karst groundwater is atmospheric precipitation and river leakage. There are a large number of coal mines in the runoff area, and the mine field area accounts for about 60%. Production activities such as mine drainage and coal processing, as well as leachate from abandoned coal mines and gangue dumps, influence the groundwater quality in the region through surface leakage and other factors.

3. Materials and Method

3.1. Sample Collection

According to the geology, landform and the distribution of coal resources of the study area, water samples, including 5 surface water samples (S1~S5), 3 gangue leachate samples (G1~G3), 5 mine water samples (M1~M5) and 17 groundwater samples, were collected in 2022. The distribution of sampling points is shown in Figure 1. Among them, surface water samples were collected from Tunlan River and Fen River, respectively, and leachate was from Tunlan Mine and Malan Mine gangue dumps, while mine water samples were collected from Tunlan, Malan, Dongqu and Xiqu Coal Mines. Pore groundwater samples (P1~P6) were taken from the civil wells in Gujiao mining area (the buried depth of groundwater of 5~20 m). Eleven karst groundwater samples (K1~K11) were collected in the recharge area, runoff area and discharge area, respectively.

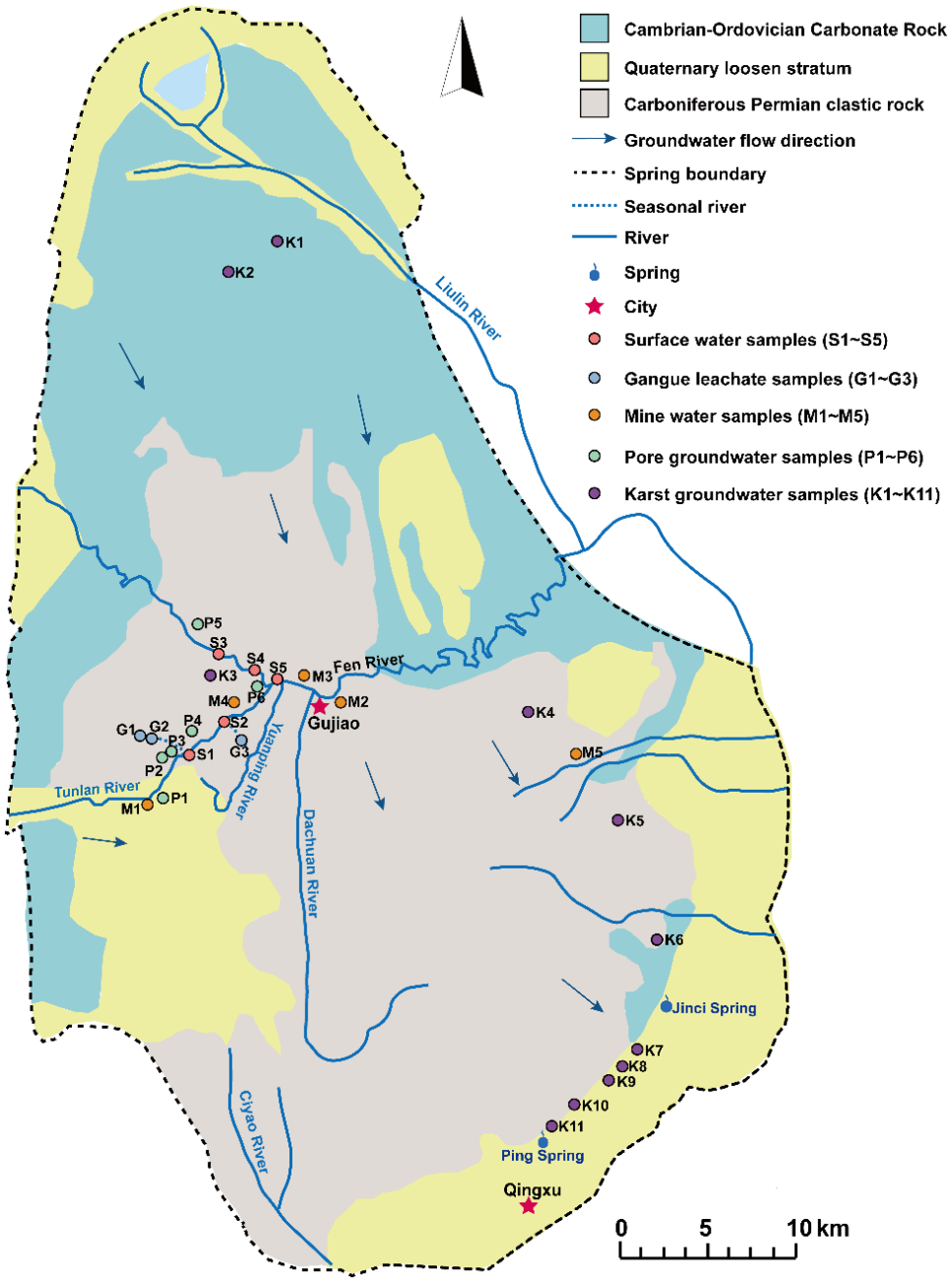

Figure 1. Study area and sampling sites.

Water samples were collected using high-density polyethylene plastic containers. Before sampling, containers were washed three times with the water to be taken, filled quickly without any headspace, sealed and quickly transported back to the laboratory for low-temperature storage for subsequent testing. The water sample used for ion analysis was filtered by a 0.45μm membrane. Sulfate in samples was completely transformed into $BaSO_4$ by the chemical precipitation method and purified and prepared as $BaSO_4$ samples by DTPA dissolution and the reprecipitation method (DDARP) [23], for isotopic mass spectrometry analysis.

3.2. Physicochemical Indicators

The position of each sampling point was evaluated by a handheld GPS locator, and the pH value and total dissolved solids (TDS) were measured in the field. The pH value was measured by a portable water quality tester (DS5, HACH, Ames, IA, USA), and the

TDS was measured by a portable detector (SX-650, Sanxin Instrumentation, Shanghai, China). The anions Cl^-, SO_4^{2-}, F^-, NH_4^+ and NO_{3-} were tested by an ion chromatograph (ICS-Aquion, Thermo, Waltham, MA, USA), and HCO_3^- and CO_3^{2-} were determined by titration [24]. K^+ and Na^+ were tested by an atomic absorption spectrophotometer (GFA-6880, Shimadzu, Kyoto, Japan), and Ca^{2+} and Mg^{2+} were tested by the EDTA titration method. Heavy metals Al, Ba, Fe and Mn were determined by inductively coupled plasma mass spectrometry (ICP-MS, TFS, Waltham, MA, USA). Sulfur isotopes ($\delta^{34}S_{SO4}$) of water samples were measured by an elemental analyzer (Flash 2000 HT, Thermo, Waltham, MA, USA) and a stable isotope mass spectrometer (Delta V, Thermo, Waltham, MA, USA) with an accuracy of less than 0.2‰. The test was completed at the Nanjing Institute of Geology and Paleontology, Chinese Academy of Sciences. Oxygen isotopes ($\delta^{18}O_{SO4}$) were measured by an elemental analyzer (Flash 2000 HT, Thermo, Waltham, MA, USA) and isotope mass spectrometer (MAT253, Thermo, Waltham, MA, USA) with an analytical accuracy of over 0.5‰ at the School of Resources and Environment of Henan Polytechnic University.

3.3. Statistical Analysis

Origin software (v. 2018) was used to draw the box plots of hydrochemical indicators and the distribution diagrams of sulfur and oxygen isotopes for the analysis of the ion-related correlations. The hierarchical clustering method based on Euclidean distance was used to cluster the distribution of sulfur and oxygen isotopes in water samples. The IsoSource model was adopted to analyze the source of sulfur and oxygen isotopes. Based on the law of mass conservation, the IsoSource model could estimate the contribution rate of various sulfate sources to groundwater sulfate pollution [25]. In this paper, the values of sulfur and oxygen isotopes from three kinds of sulfate sources in groundwater were input to establish the mass conservation model. The tolerance parameters and incremental parameters of the model were set, and the percentages of sulfate from different sources were calculated by an iterative method. Only when the difference between sulfur and oxygen isotopes from different sources and those in water samples was less than 0.1% could the solution be considered possible.

$$\delta^{34}S_{SO4} = f_1 \times \delta^{34}S_1 + f_2 \times \delta^{34}S_2 + f_3 \times \delta^{34}S_3 \quad (1)$$

$$\delta^{18}O_{SO4} = f_1 \times \delta^{18}O_1 + f_2 \times \delta^{18}O_2 + f_3 \times \delta^{18}O_3 \quad (2)$$

$$f_1 + f_2 + f_3 = 1 \quad (3)$$

where f_1, f_2 and f_3 represent the proportion of different sulfate pollution sources, %; $\delta^{34}S_1$, $\delta^{34}S_2$ and $\delta^{34}S_3$ represent sulfur isotope values from different sources, ‰; $\delta^{18}O_1$, $\delta^{18}O_2$ and $\delta^{18}O_3$ represent oxygen isotope values from different sources, ‰; and $\delta^{34}S_{SO4}$ and $\delta^{18}O_{SO4}$ represent the isotopic values of sulfur and oxygen of the water sample.

4. Results and Discussion

4.1. Physicochemical Parameters of Samples

Physicochemical parameters of the water samples are shown in Table 1. The pH values of surface water, pore groundwater and karst groundwater were 7.97~8.55, 7.63~8.20 and 7.80~8.39, respectively, indicating weakly alkaline, while the gangue leachate and mine water samples were acidic or nearly neutral, with the lowest pH values of 3.22 and 4.72, respectively. As the comprehensive index of water samples, the TDS of pore groundwater and karst groundwater in the study area was 550.00~1760.00 and 248.00~2180.00 mg/L, respectively. Compared with the level III limit of groundwater quality standard (1000.00 mg/L) [26], 58.82% of the TDS in groundwater exceeded the standard, indicating that the groundwater may have been contaminated. The average SO_4^{2-} concentrations of pore groundwater and karst groundwater were 504.01 and 598.94 mg/L, respectively. A total of 64.70% of groundwater exceeded the level III limit of standard (250 mg/L) [26], and the highest SO_4^{2-} concentration reached 2000 mg/L. The average SO_4^{2-} concentrations of gangue leachate and mine water were 4282.00 and 1407.59 mg/L, respectively,

and the higher concentration of sulfate may mainly derive from the oxidation of sulfide minerals (mainly pyrite) during acid production. The oxidation of pyrite leads to a decrease in pH, while releasing large amounts of sulfate, iron and manganese [27]. The highest concentrations of Fe, Mn and sulfate in gangue leachate were 690.00, 53.50 and 6637.00 mg/L, respectively. The high concentration of sulfate in the gangue leachate may enter the groundwater system through surface infiltration, leading to the increase in SO_4^{2-} in the groundwater. Therefore, it is necessary to use sulfur–oxygen isotopes of sulfate to trace the pollution sources in the study area.

Table 1. Statistics of physicochemical parameters of different group samples.

Number	Surface Water			Gangue Leachate			Mine Water			Pore Groundwater			Karst Groundwater		
	Min	Max	Average	Min	Max	Average	Min	Max	Average	Min	Max	Average	Min	Max	Average
PH	7.97	8.55	-	3.22	6.54	-	4.72	7.89	-	7.63	8.20	-	7.80	8.39	-
TDS	597	1200	790.80	2940	7200	4646.67	1680	3530	2232.00	550	1760	1253.33	248.00	2180.00	950.91
K^+	2.89	4.06	3.29	7.31	25.63	17.38	3.23	8.73	5.61	1.53	4.62	3.05	0.63	7.98	2.36
Na^+	53.08	155.76	83.05	584.75	765.41	677.77	229.85	461.01	358.46	29.40	128.86	92.79	11.60	130.00	38.81
Ca^{2+}	61.89	127.75	86.29	21.70	281.26	109.42	99.39	329.44	211.88	81.67	299.70	205.93	53.80	216.00	115.45
Mg^{2+}	29.32	34.28	31.11	27.19	101.12	61.41	30.87	227.50	103.05	26.56	81.74	63.33	23.90	95.00	54.75
Cl^-	49.95	134.95	80.10	61.80	82.80	74.03	41.19	306.71	141.44	22.35	151.17	100.20	12.27	46.20	32.32
SO_4^{2-}	114.01	393.90	216.83	2029.00	6637.00	4282.00	449.06	3015.38	1407.59	87.26	850.37	504.01	28.60	2000.00	598.94
CO_3^{2-}	4.71	14.12	9.89	0.00	1.00	0.33	0.00	0.00	0.00	0.00	9.42	1.57	0.00	0.00	0.00
HCO_3^-	208.21	277.61	236.21	0.00	59.40	19.80	0.00	569.59	261.34	253.68	409.24	343.02	78.00	331.00	204.50
F^-	0.48	0.84	0.62	1.32	2.09	1.77	0.50	3.83	1.71	0.38	0.67	0.51	-	-	-
NH_4^+	0.11	1.06	0.49	-	-	-	0.20	8.90	2.52	0.00	5.28	1.32	-	-	-
NO_3^-	2.69	19.23	7.11	-	-	-	0.00	1.94	0.84	18.96	96.15	42.94	-	-	-
Al	0.06	0.21	0.11	0.04	37.60	23.88	0.02	75.50	15.16	0.01	0.03	0.02	-	-	-
Ba	0.06	0.13	0.10	32.50	45.70	40.77	0.02	0.07	0.05	0.04	0.20	0.09	-	-	-
Fe	0.06	0.57	0.18	0.03	690.00	279.68	0.12	34.20	7.28	0.02	0.04	0.03	0.00	2.03	-
Mn	0.00	0.20	0.05	5.61	53.50	27.44	0.12	17.40	4.69	4.63	10.00	7.32	0.00	1.49	-

Note: Unit mg/L.

The concentrations of F^-, NH_4^+ and NO_3^- in pore groundwater ranged from 0.38 to 0.67, 0.00 to 5.28 and 18.96 to 96.15 mg/L, respectively. The standard limits of NH_4^+ and NO_3^- in groundwater were 1.50 and 30.00 mg/L, respectively. However, the NH_4^+ concentrations in pore groundwater P2 and P3 were 2.66 and 5.28 mg/L, respectively, and the NO_3^- concentrations in P2, P5 and P6 were 32.01, 64.28 and 96.15 mg/L, respectively, which all exceeded the standard limits. The NH_4^+ and NO_3^- in groundwater were mainly from anthropogenic sources, indicating that the pore water in the study area may have been contaminated by agricultural irrigation or domestic wastewater [28]. The concentrations of Mn in pore groundwater P2 and P3 were relatively high, 4.63 and 10.00 mg/L, respectively, which seriously exceeded the standard limit (1.5 mg/L). The higher concentration of Mn in the pore groundwater may mainly derive from the surface infiltration of gangue leachate. As illustrated in Figure 1, P2 and P3 are distributed downstream of gangue leachate (G1 and G2). The content of Mn in gangue leachate G2 was as high as 53.5 mg/L due to the influence of acid production of gangue oxidation, and this contaminated water may enter the groundwater system through surface infiltration, leading to the increase in Mn content in downstream pore groundwater. The Fe and Mn concentrations in karst groundwater K8 and K9 were 0.60 and 2.03 mg/L, with 1.49 and 0.10 mg/L, respectively. The higher Fe and Mn concentrations in karst groundwater K8 and K9 may be attributed to the influence of acidic water infiltration from abandoned coal mines near Huanglou Village [29].

Figure 2 indicates the main hydrochemical indexes of karst groundwater in different areas of the study area. The average concentrations of TDS, SO_4^{2-}, Ca^{2+} and Mg^{2+} in karst groundwater in the recharge area (K1~K2) are 269.50, 31.8, 57.6 and 24.55 mg/L, respectively. Both TDS and SO_4^{2-} could meet the level I standard of groundwater. There are multiple coal mines and coal processing industrial sites in the runoff area of karst groundwater. With the infiltration of surface pollution, the TDS content of karst groundwater (K3~K6) gradually increased (with an average of 620.25 mg/L), and the average contents of Ca^{2+}, Mg^{2+} and SO_4^{2-} increased to 1.68, 2.00 and 9.26 times that of the recharge area, respectively. The SO_4^{2-} contents of K5 and K6 have exceeded the level V limit (350 mg/L) of groundwater. As shown in Figure 2, the chemical indexes of karst groundwater (K7~K11) in the drainage area

were further increased, with the average contents of TDS, Ca^{2+}, Mg^{2+} and SO_4^{2-} of 1488.00, 153.60, 71.36 and 1069.2 mg/L, respectively. The average SO_4^{2-} concentration increased to 33.62 times that of the recharge area. The karst groundwaters in all charge areas exceeded the level V standards of groundwater, with a concentration of up to 2000.00 mg/L in Niujiaokou Village (K7). On the whole, the TDS and main ion contents in karst groundwater are increasing gradually from the recharge area and runoff area to the discharge area, which is consistent with the trend of changes in the hydrochemical indexes of karst groundwater in the region over the years [30,31]. The results of groundwater quality evaluation show that the karst groundwater was level II and level IV water in the runoff area and drainage area in 2015, respectively [30]. However, with the gradual increase in groundwater pollution, the water quality has exceeded the Class V limit, indicating a deteriorating trend in the water quality of karst groundwater in the Jinci Spring area.

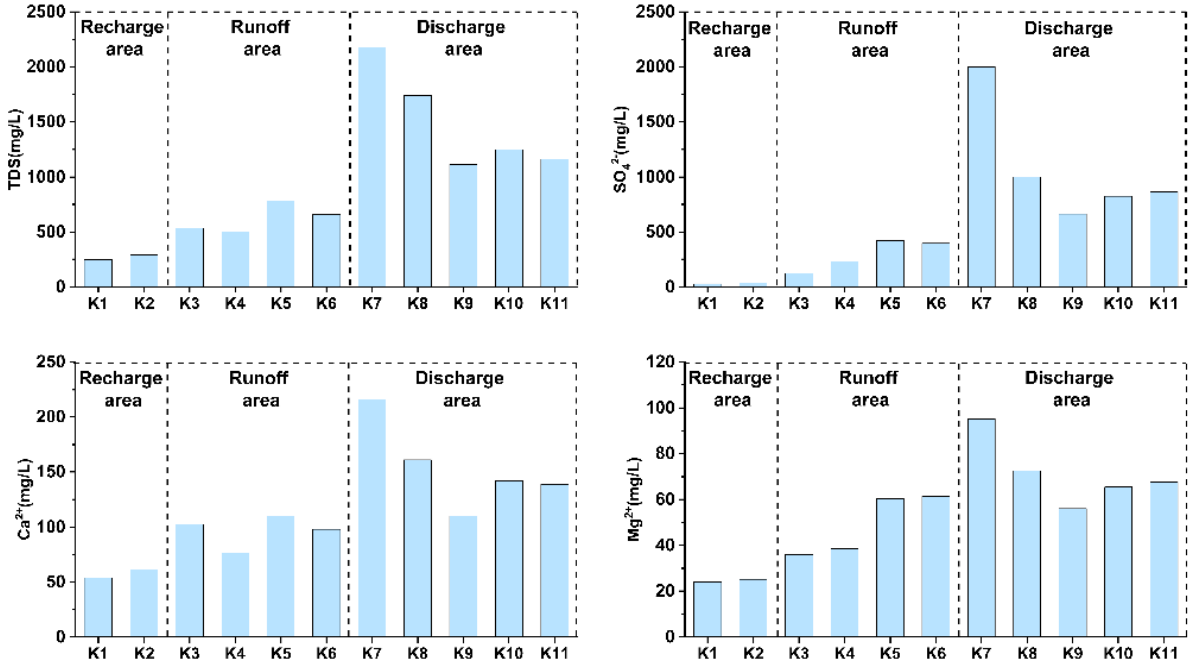

Figure 2. Distribution of TDS, SO_4^{2-}, Ca^{2+} and Mg^{2+} in karst groundwater samples.

4.2. Hydrochemical Characteristics of Samples

Since the hydrochemical characteristics of regional surface and groundwater can be influenced by geological conditions, hydrodynamic conditions and human engineering activities, this complex information can be better inverted by analyzing the hydrochemical characteristics of karst groundwater [32,33]. The Piper diagram is an important tool to study the characteristics of hydrochemical types and can reflect the distribution of main anions and cations (Figure 3). The anions in surface river water (Group S) were mainly SO_4^{2-} and HCO_3^-, and the main cations were Ca^{2+}, Na^+ and Mg^{2+}. According to the Shukalev classification [34], the main hydrochemical types were SO_4·HCO_3-Ca·Na and SO_4·HCO_3-Ca·Na·Mg·SO_4^{2-} that dominated in the anions of gangue leachate, accounting for 96.61% on average, and the hydrochemical types were SO_4-Na and SO_4-Ca·Na. The distribution of ions was discrete in the mine water of different coal mines, which may be related to differences in coal seams and production conditions. Among them, SO_4^{2-} in M3 and M5 was up to over 90%, and the hydrochemical type was SO_4-Ca·Na·Mg. The hydrochemical types of other mine water were SO_4·HCO_3-Na (M1), SO_4-Ca·Na (M2) and SO_4·Cl-Na (M4). The main anions of pore groundwater were SO_4^{2-} and HCO_3^-, and the main cations were Ca^{2+} and Mg^{2+}. The pore groundwater (P2 and P3) near Jijiazhuang Village had high contents of Ca^{2+} and SO_4^{2-}, its hydrochemical type was SO_4-Ca and the hydrochemistry of other pore groundwater was SO_4·HCO_3-Ca·Mg. SO_4^{2-} in pore groundwater may derive

from the dissolution of gypsum minerals or surface infiltration. There are gangue dumps upstream of Jijiazhuang Village, so the infiltration of high-concentration sulfate in leachate from gangue may be the reason for the dominance of SO_4^{2-} in P2 and P3. Ca^{2+} and Mg^{2+} are the main cations in karst groundwater, with average percentages of 48.71% and 38.23%, respectively, while the distribution of anions was different. HCO_3^- was the main anion in the karst groundwater (K1 and K2) in the recharge area, and the hydrochemical type is HCO_3-Ca·Mg. Affected by the dissolution of sulfur-bearing minerals in coal-bearing strata, mine drainage and human activities, the proportion of SO_4^{2-} in karst groundwater in the runoff area gradually increased from 13.64% to the highest at 89.91%, and the proportion of HCO_3^- gradually decreased from 71.33% to 7.78%. Meanwhile, the hydrochemical types in the runoff area also evolved into SO_4·HCO_3-Ca·Mg. SO_4^{2-} was the main anion in the karst groundwater in the drainage area, accounting for more than 80%, so the hydrochemical type also changed to SO_4-Ca·Mg.

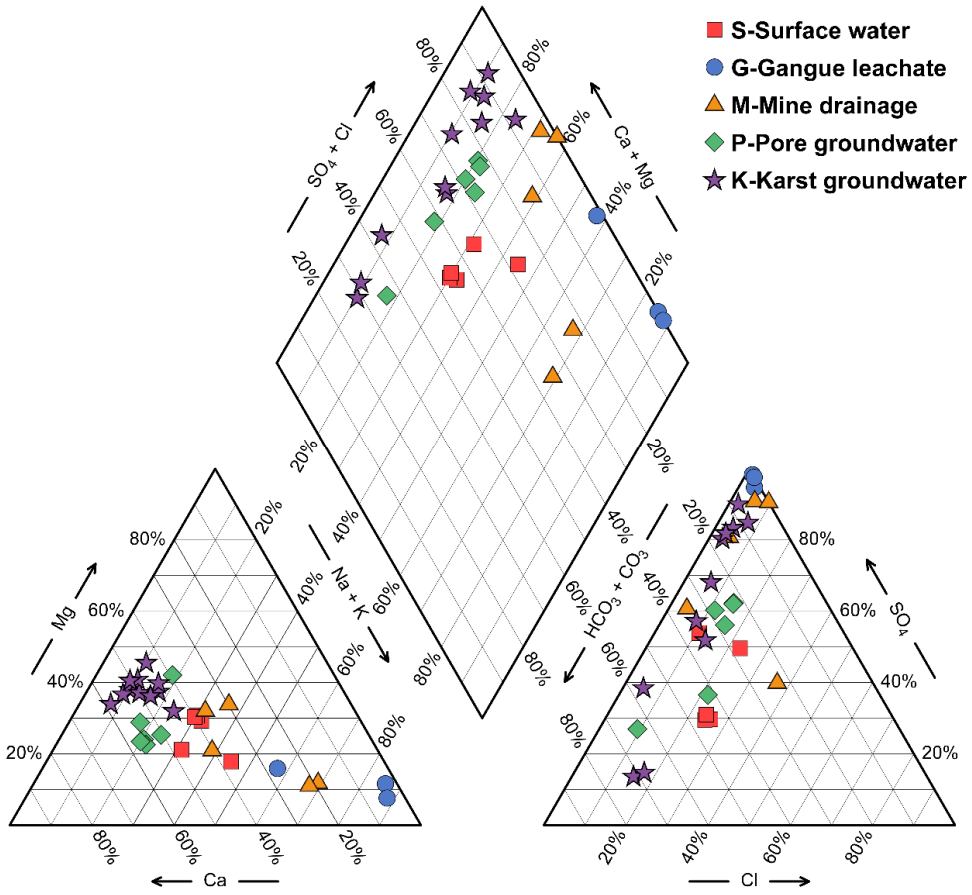

Figure 3. Distribution and hydrochemical characteristics of different types of water samples.

4.3. Analysis of Water–Rock Interaction of Water Samples

TDS of water samples in the study area was highly correlated with SO_4^{2-}, with a correlation coefficient of 0.969, indicating that SO_4^{2-} was the main factor affecting the overall indicators of water quality. Therefore, the analysis of sulfate sources can be used to judge the attribution of regional water pollution. According to Figure 4a, the increasing trend of SO_4^{2-} concentration and TDS in regional surface water, pore groundwater and karst groundwater samples are the same as those in mine water and leachate from gangue, so it can be inferred that mine water and gangue leachate may impact the water quality of surface water and groundwater at the same time [35]. According to the relationship between Ca^{2+} and SO_4^{2-}, the degree of the impact of gypsum dissolution on regional groundwater can be judged. If the groundwater is significantly affected by gypsum dissolution, the

dissolved components in groundwater should be close to the gypsum dissolution line. It can be seen from Figure 4b that the pore groundwater is basically distributed near the gypsum dissolution line, indicating that gypsum dissolution has an obvious influence on pore groundwater. Karst groundwater (K1~K3) is slightly distributed below the gypsum dissolution line, indicating that Ca^{2+} cannot be balanced by SO_4^{2-}. One reason is that there may be other potential sources of Ca^{2+}, such as the dissolution of calcite and dolomite, and the other reason is that the concentration of Ca^{2+} in the surface recharge water may be slightly higher than that of SO_4^{2-} since these three types of karst groundwater were highly influenced by the recharge of surface water. Other samples of karst groundwater, mine water and gangue leachate are all distributed above the gypsum dissolution line, indicating that SO_4^{2-} still has other sources, such as artificial input or pyrite dissolution.

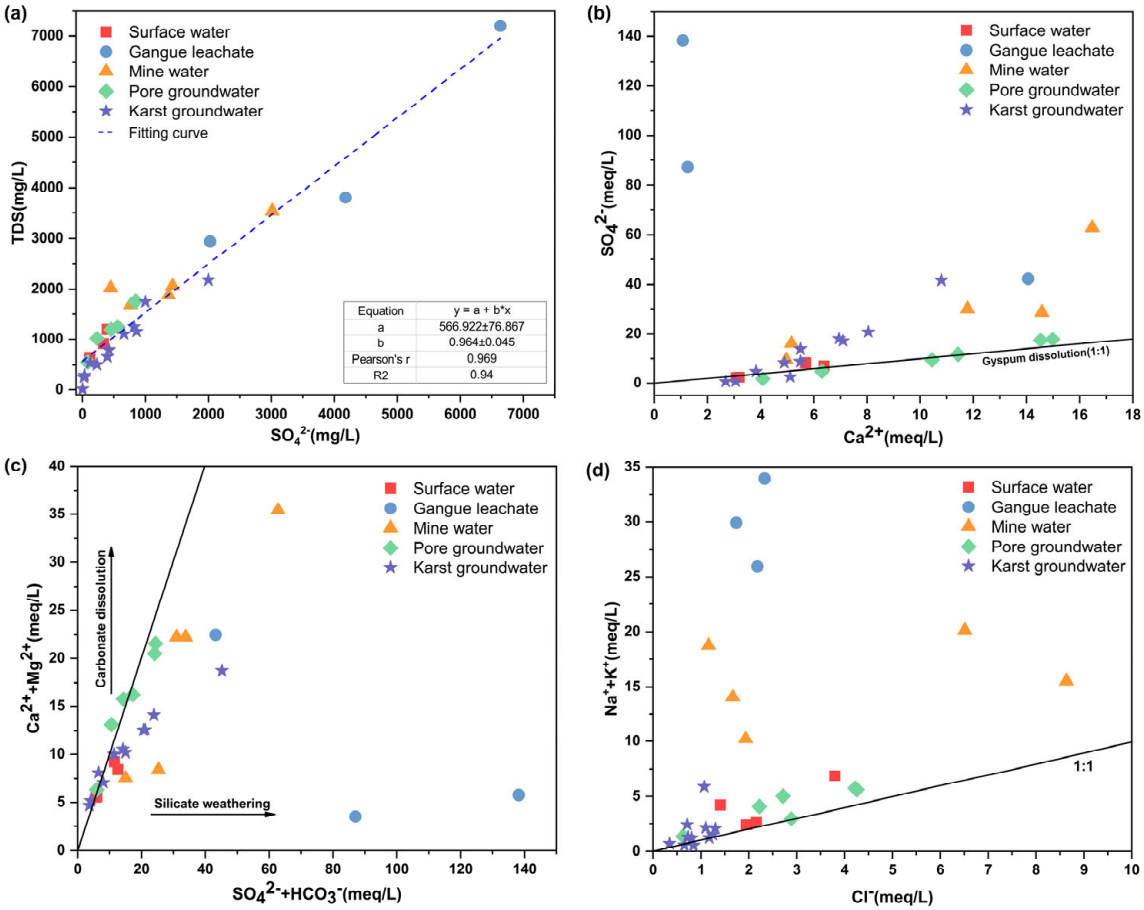

Figure 4. Ionic relationships of water samples in the study area. (**a**) TDS vs. SO_4^{2-}; (**b**) SO_4^{2-} vs. Ca^{2+}; (**c**) Ca^{2+} + Mg^{2+} vs. SO_4^{2-} + HCO_3^-; (**d**) Na^+ + K^+ vs. Cl^-.

The ratio of (Ca^{2+} + Mg^{2+})/(SO_4^{2-} + HCO_3^-) can be used to determine the source of Ca^{2+}, Mg^{2+}, SO_4^{2-} and HCO_3^- [36]. As shown in Figure 4c, K1, K2 and P1 are basically distributed near the equilibrium line, indicating that the groundwater composition is mainly controlled by water–rock interaction. The leachate from gangue, mine water and karst groundwater (K5~K11) is located at the lower right of the equilibrium line, indicating that the decrease in equivalent concentrations of Ca^{2+} and Mg^{2+} or the increase in SO_4^{2-} and HCO_3^- in groundwater may be related to cation exchange or artificial input of SO_4^{2-} and organic matter. This is basically consistent with the conclusion of the analysis in Figure 4b. Karst groundwater K4 and pore groundwater P5 are slightly above the equilibrium line, which may be related to the reverse cation exchange or sulfate bacteria reduction process [36]. Salt rock dissolution is an important source of Na^+ and Cl^- in groundwater. In Figure 4d, it can be seen that all the samples except K1 and K2 are slightly

below the salt rock dissolution line, which indicates that Na^+ in groundwater cannot be balanced by Cl^-, which may be due to ion exchange between Na^+, Ca^{2+} and Mg^{2+} [37] or other sources of Na^+, such as human input.

4.4. Distribution of Sulfur and Oxygen Isotopes in Water Samples

The ranges of $\delta^{34}S_{SO4}$ and $\delta^{18}O_{SO4}$ values of 30 water samples in the study area were 10.01 to +24.42‰ and −4.90 to +12.40‰, respectively. At the same time, sulfur and oxygen isotope data of three local atmospheric precipitation samples of Taiyuan were collected as the control group (Figure 5a). The hierarchical clustering results based on Euclidean distance show that the water samples in the study area can be grouped into three clusters (Figure 5b). Cluster I is mainly distributed in the center of Figure 5a, the $\delta^{34}S_{SO4}$ value ranges from −2.77 to 6.71‰ and $\delta^{18}O_{SO4}$ ranges from 0.50 to 5.50‰. Surface water, atmospheric precipitation and some groundwater samples were distributed in this area. Cluster II is mainly distributed at the lower left of Figure 5a. $\delta^{34}S_{SO4}$ of these points ranges from −10.01 to −3.95‰, and $\delta^{18}O_{SO4}$ ranges from −4.90 to 1.40‰. Leachate from gangue, part of the mine water and pore groundwater (P2~P4) and karst groundwater (K5, K7) were distributed in the area, and they have relatively negative sulfur and oxygen isotopes. The increase in gypsum input ratio and the reduction in sulfate bacteria could cause the positive values of $\delta^{34}S_{SO4}$ and $\delta^{18}O_{SO4}$ at the same time, while the increase in sulfide mineral input ratio can lead to the negative values of $\delta^{34}S_{SO4}$ and $\delta^{18}O_{SO4}$ [38]. Therefore, the SO_4^{2-} at these points may mainly derive from the oxidation of sulfide minerals. Cluster III is mainly distributed in the upper right, with $\delta^{34}S_{SO4}$ and $\delta^{18}O_{SO4}$ values ranging from 14.16 to 24.42‰ and 2.40 to 12.40‰, respectively. The sulfur and oxygen isotopes of these samples are all positive, on the one hand, probably because their sulfates may mainly derive from gypsum dissolution, and on the other hand, possibly because of the fractionation effect of the sulfate bacterial reduction process, which led to the increase in sulfur–oxygen isotope values.

The potential sources of sulfate include atmospheric precipitation, rock weathering (gypsum dissolution and pyrite oxidation) and human factors [39]. Sulfates from different sources have different $\delta^{34}S_{SO4}$ values. In this study, three atmospheric precipitation samples were collected in Taiyuan area, and sulfur and oxygen isotopes were analyzed. The range of $\delta^{34}S_{SO4}$ values was 2.41 to 3.83‰, mainly distributed in the central area of Figure 5c. Marine sedimentary gypsum minerals usually have high $\delta^{34}S_{SO4}$ composition. The $\delta^{34}S_{SO4}$ value of Precambrian gypsum is as high as 31‰, and the $\delta^{34}S_{SO4}$ value of Handan Middle Ordovician gypsum is in the range of 20 to 24‰ [40]. The $\delta^{34}S_{SO4}$ value of the Middle Ordovician gypsum in Shanxi is 23.8~31.4‰ [41]. In this study, some karst groundwaters (K3, K6, K9, K10 and K11) were distributed in the upper right area, and the range of $\delta^{34}S_{SO4}$ was 19.61 to 24.42‰. Sulfate in these samples may mainly derive from the dissolution of gypsum minerals. The composition of $\delta^{34}S_{SO4}$ in sedimentary rock pyrite is usually low; for example, pyrite in coal seams of different regions of China ranges from 3.4‰ to 10.2‰ for $\delta^{34}S_{SO4}$ [42], and $\delta^{34}S_{SO4}$ values of magmatic pyrite range from −5‰ to +5‰ [40,43]. The sulfur isotope is not obviously fractionated during pyrite oxidation, so the content of $\delta^{34}S_{SO4}$ in sulfate formed by oxidation is similar to that of pyrite, and some studies show that the $\delta^{34}S_{SO4}$ value in pyrite oxide is −15~4‰ [44]. According to Figure 4c, the samples of leachate from gangue, mine water, pore groundwater and some karst groundwaters (K5, K7 and K8) are all distributed in the lower right, and the $\delta^{34}S_{SO4}$ values of these samples are mostly negative, so SO_4^{2-} in these samples may mainly derive from the oxidation of pyrite.

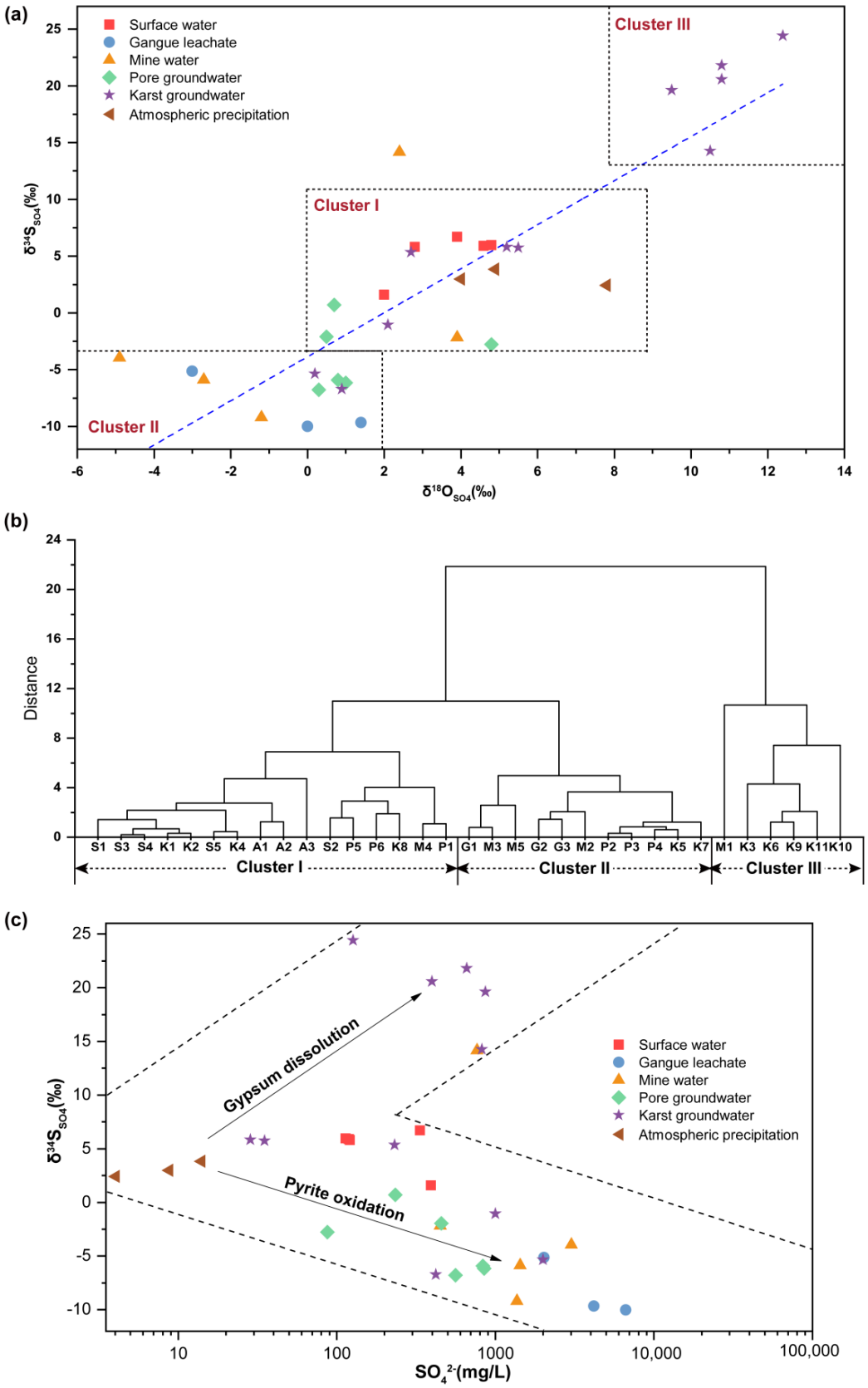

Figure 5. Distribution of $\delta^{34}S_{SO4}$ and $\delta^{18}O_{SO4}$ in different types of water samples (**a**). Clustering of sulfur and oxygen isotopes among samples (**b**). Distribution of SO_4^{2-} and $\delta^{34}S_{SO4}$ in water samples indicates the possible source of sulfate (**c**).

4.5. Identification of Groundwater Contamination Sources Based on Sulfur Isotopes

Sulfates from different potential sources in groundwater have different compositions of $\delta^{34}S_{SO4}$ and $\delta^{18}O_{SO4}$. This study calculated the contribution rates of sulfate sources to groundwater sulfate pollution by IsoSource model [25]. The calculation had considered the input of sulfide mineral (pyrite) oxidation, atmospheric precipitation and gypsum dissolution to the groundwater and surface water sulfate. Figure 6 shows the calculation results. SO_4^{2-} from gypsum dissolution, atmospheric precipitation and pyrite oxidation in surface water was 20%~36% (average 31%), 2.0%~6.8% (4%) and 61%~73.3% (64%), respectively, with pyrite oxidation being the main source of sulfate in surface water. Sulfate produced by pyrite oxidation mainly comes from mine water and leachate from gangue, indicating that the surface rivers in Xishan mining area have been polluted by coal-related industrial sites to varying degrees. SO_4^{2-} produced by pyrite oxidation in pore groundwater accounted for 44.50%~95.30% (81% on average), which may be due to the infiltration of mine water or gangue leachate through the surface or rock cracks, resulting in pore groundwater pollution. In particular, P2, P3 and P4 directly affected by gangue dumps had higher proportions of pyrite oxidation, exceeding 88% at a single point. Pore groundwater P1 was highly influenced by atmospheric precipitation infiltration (54%), while sulfates in P5 and P6 pore groundwater derive from the dissolution of gypsum minerals (accounting for 18% and 12%, respectively).

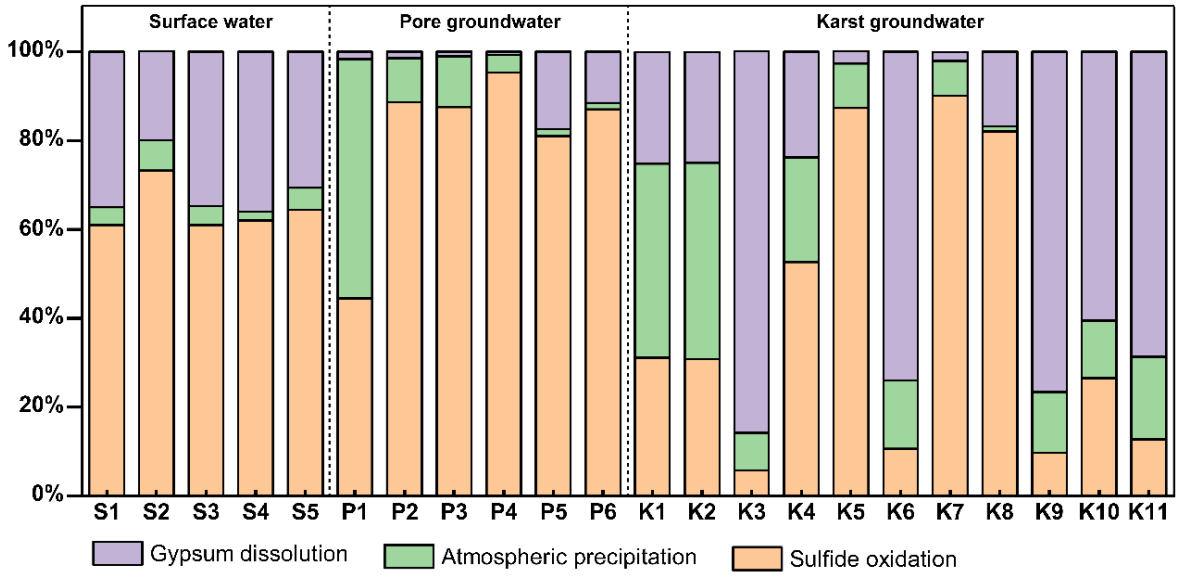

Figure 6. Explanation of sulfate sources in surface and groundwater samples in the study area based on sulfur isotope calculations.

The proportion of sulfate from dissolved gypsum, atmospheric precipitation and pyrite oxidation sources in karst groundwater ranged from 1.9% to 85.9%, 1.3% to 44.2% and 5.7% to 90.1%, respectively, with significant differences among karst groundwater samples (Figure 6). The percentages of sulfate in karst groundwater K1 and K2 from gypsum dissolution, atmospheric precipitation and pyrite oxidation were25%, 44% and 31%, respectively, indicating that karst group of the recharge area was significantly influenced by atmospheric precipitation. The karst groundwater in K3 and K6 in the runoff area was mainly influenced by the dissolution of the Ordovician gypsum interlayer (86% and 74%, respectively), while SO_4^{2-} of K4 and K5 was mainly influenced by the oxidation of pyrite (53% and 87%, respectively), and in addition, karst groundwater K4 was also affected by the infiltration of atmospheric precipitation (24%). The concentration of SO_4^{2-} in karst groundwater of the discharge area ranged from 660 to 2000 mg/L. It can be seen that sulfate in K9 and K10 samples mainly came from gypsum dissolution, accounting for 77%, 61%

and 69%, respectively. The concentrations of sulfate in K7 and K8 are as high as 2000 and 1000 mg/L, respectively, and the source analysis results indicate that they may be mainly from pyrite oxidation, accounting for up to 90% and 82%, respectively. This may be due to the rebound of groundwater to the mining area after the abandonment of the coal mines near K7 and K8 to form acid mine water [29], which later caused cascading contamination of karst groundwater through channels such as rock fissures.

4.6. Temporal Variation of Sulfate Pollution in the Jinci Spring Area

The concentration of SO_4^{2-} in karst groundwater samples in the Jinci Spring area ranged from 53.8 to 919 mg/L in the year of 1989, with $\delta^{34}S_{SO4}$ values ranging from −0.33 to +37.00‰ [45]. The $\delta^{34}S_{SO4}$ values of karst groundwater were positive (+8.2~+37.0‰) except for samples collected from Getashang village. In 2016, Tang et al., carried out sulfur isotope analysis of karst water in the drainage area of the Bianshan fracture zone in the Jinci Spring domain and found that the SO_4^{2-} concentration range of karst water was 35.00 to 1221.51 mg/L, with a $\delta^{34}S_{SO4}$ range of +8.21‰ to +25.84‰ [46]. Gypsum minerals usually have a high $\delta^{34}S_{SO4}$ composition [40]. In 1989 and 2016, the sulfate of karst groundwater in the Jinci Spring area was mainly distributed in the upper right area (Figure 7). Therefore, it is speculated that sulfate may mainly derive from the dissolution of gypsum minerals. Results of the measurements in 2022 showed that the range of SO_4^{2-} concentration in the karst groundwater of the Jinshi spring domain was 28.26 to 200.000 mg/L, with the range of $\delta^{34}S_{SO4}$ of −6.72‰ to +24.42‰. Compared with 1989 and 2016, the $\delta^{34}S_{SO4}$ values of some karst groundwater were significantly decreased. The values of $\delta^{34}S_{SO4}$ in pyrite oxide usually range from −15‰ to 4‰ [44]. The $\delta^{34}S_{SO4}$ values of K5, K7 and K8 were −6.72‰, −5.36‰ and −1.06‰, respectively, which was likely due to the pyrite oxidation dissolution. The coal production activities have led to the gradual oxidation and dissolution of pyrite in coal strata and gangue and infiltration to groundwater, resulting in the expansion of karst water pollution in the Xishan mining area in terms of time change.

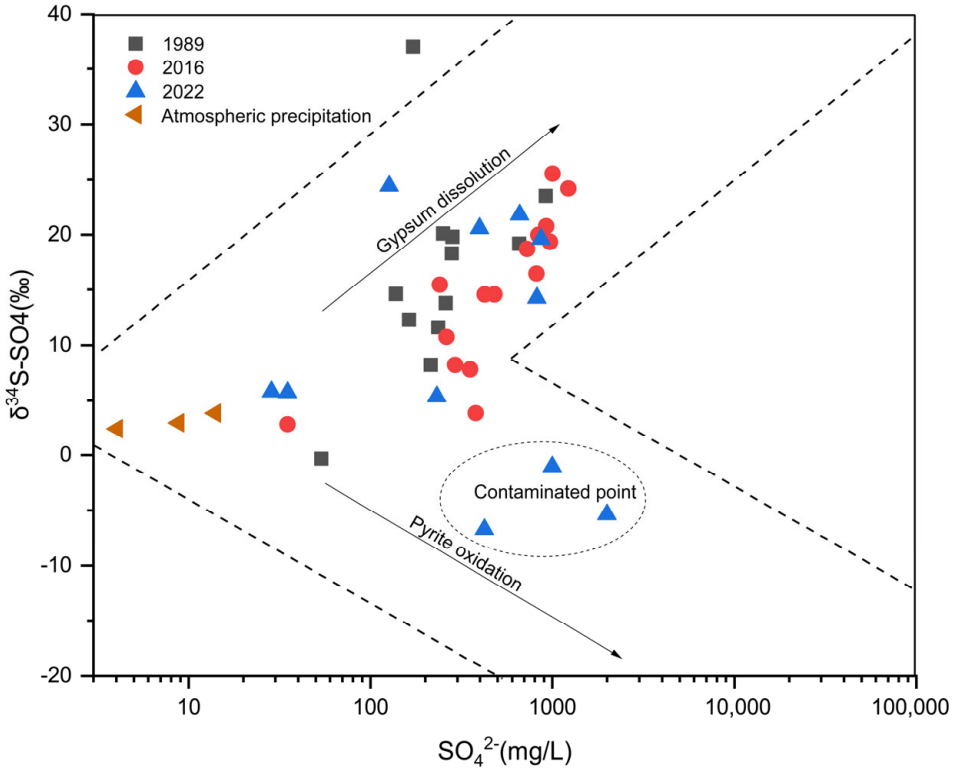

Figure 7. Distribution of $\delta^{34}S_{SO4}$ and SO_4^{2-} in karst groundwater of the Jinci Spring area of different years.

5. Conclusions

In this study, Xishan mining area, a typical coal-related industrial cluster in Northern China, was selected as the research area. Through the analysis of hydrochemical characteristics and sulfur and oxygen isotopes of surface water and groundwater in the region, the hydrochemical characteristics and pollution causes were revealed. It was found that due to the influence of the coal industry, TDS in 58.82% of groundwater exceeded the standard in Xishan mining area, sulfate in 64.7% of groundwater exceeded the standard, and the quality of some karst groundwaters exceeded the Class V limit of groundwater, up to 2000 mg/L, showing a deteriorating trend of the groundwater quality. The proportion of SO_4^{2-} artificially input into karst groundwaters increased in the runoff area and discharge area. The hydrochemical type of karst groundwater gradually changed from HCO_3-Ca·Mg type to SO_4-Ca·Mg type from the recharge area to discharge area.

The range of $\delta^{34}S_{SO4}$ and $\delta^{18}O_{SO4}$ values of water samples in the study area were −10.01 to +24.42‰ and −4.90 to +12.40‰, respectively. The sulfur and oxygen isotope values of gangue leachate, mine water and part of karst groundwaters were close to the dissolved end members of sulfide minerals, indicating that the sulfates mainly derive from sulfide minerals (FeS_2) in coal and gangue, particularly the oxidation of pyrite. The sources of sulfate in surface water and groundwater were analyzed by using the IsoSource model. The results showed that sulfate in surface water mainly came from pyrite oxidation (64% on average) and gypsum dissolution (31%), and pore groundwater mainly came from pyrite oxidation (81%). The karst groundwater in the recharge area was greatly influenced by atmospheric precipitation recharge, and the proportion of sulfate in some karst groundwater was significantly increased (up to 90%), affected by pyrite oxidation in the runoff area and drainage area. Comparing the distributions of sulfur and oxygen isotopes in karst groundwaters in the study area over the years, it was found that $\delta^{34}S_{SO4}$ in some areas decreased significantly in 2022, towards the dissolved end members of sulfide minerals, and the pollution range of karst groundwater in Xishan mining area has expanded. Therefore, it is necessary to control groundwater pollution in Xishan mining area.

Author Contributions: Conceptualization, D.C. and Q.F.; Formal analysis, D.C.; Funding acquisition, Q.F.; Investigation, D.C. and M.G.; Methodology, D.C.; Software, M.G.; Supervision, Q.F.; Validation, D.C.; Writing—original draft, D.C.; Writing—review and editing, Q.F. and M.G. All authors have read and agreed to the published version of the manuscript.

Funding: This research was funded by the Key Technologies Research and Development Program of China (grant No. 2020YFC1806501) and National Natural Science Foundation of China (No. 41977159).

Data Availability Statement: Not applicable.

Acknowledgments: The authors would like to thank the financial support from Key Technologies Research and Development Program of China (grant No. 2020YFC1806501) and National Natural Science Foundation of China (No. 41977159). Further thanks to Lei Meng, Xin Zhang and Yanqing Rong for their valuable help on the collection of samples.

Conflicts of Interest: The authors declare no conflict of interest.

References

1. Yuan, L. Comprehensive development and utilization of abandoned mine resources, help achieve the goal of "emission peak and carbon neutralization". *Sci. Technol. Rev.* **2021**, *39*, 1.
2. Li, J.Y.; Wang, J.M. Comprehensive utilization and environmental risks of coal gangue: A review. *J. Clean. Prod.* **2019**, *239*, 117946. [CrossRef]
3. Feng, Q.Y.; Zhou, L. *Risk Assessment and Control of Groundwater Pollution in Abandon Mine*; China Environmental Science Press: Beijing, China, 2016.
4. Smith, D.N.I.; Ortega-Camacho, D.; Acosta-González, G.; Leal-Bautista, R.M.; Fox, W.E.; Cejudo, E. A multi-approach assessment of land use effects on groundwater quality in a karstic aquifer. *Heliyon* **2020**, *6*, e3970. [CrossRef] [PubMed]
5. Sheibani, S.; Ataie-Ashtiani, B.; Safaie, A.; Simmons, C.T. Influence of lakebed sediment deposit on the interaction of hypersaline lake and groundwater: A simplified case of lake Urmia, Iran. *J. Hydrol.* **2020**, *588*, 125110. [CrossRef]

6. Huo, J.Y.; Yu, S.; Zhang, Q.H.; Li, L. Hydrochemical characteristics and estimation of the dissolved inorganic carbon flux in the Donghe River Basin of western Hunan. *Hydrogeol. Eng. Geol.* **2019**, *46*, 64–72.
7. Zhou, J.X.; Ding, Y.J.; Zeng, G.X.; Wu, J.K.; Qin, J. Major ion chemistry of surface water in the upper reach of Shule River basin and the possible controls. *Environ. Sci.* **2014**, *35*, 3315–3324.
8. Li, J.; Zou, S.Z.; Zhao, Y.; Zhao, R.K.; Dang, Z.W.; Pan, M.Q.; Zhu, D.N.; Zhou, C.S. Major ionic characteristics and factors of karst groundwater at Huixian karst wetland, China. *Environ. Sci.* **2021**, *42*, 1750–1760.
9. Sappa, G.; Vitale, S.; Ferranti, F. Identifying Karst Aquifer Recharge Areas using Environmental Isotopes: A Case Study in Central Italy. *Geosciences* **2018**, *8*, 351. [CrossRef]
10. Wannous, M.; Theilen-Willige, B.; Troeger, U.; Falk, M.; Siebert, C.; Bauer, F. Hydrochemistry and environmental isotopes of spring water and their relation to structure and lithology identified with remote sensing methods in Wadi Araba, Egypt. *Hydrogeol. J.* **2021**, *29*, 2245–2266. [CrossRef]
11. Gu, H.B.; Chi, B.M.; Wang, H.; Zhang, Y.W.; Wang, M.Y. Relationship between surface water and groundwater in the Liujiang basin-hydrochemical constrains. *Adv. Earth Sci.* **2017**, *32*, 789–799.
12. Liu, B.; Wang, H.; Jiang, Y.H.; Jia, Y.F.; Yang, Y.; Gu, H.B.; Huan, H. Transformation relationship of different water body in Donggong River basin based on hydrochemistry. *Res. Environ. Sci.* **2020**, *33*, 1979–1990.
13. Nguyen, B.C.; Putaud, J.P. Stable isotopes: Natural and anthropogenic sulphur in the environment. *Atmos. Res.* **1993**, *29*, 275. [CrossRef]
14. Tuttle, M.; Breit, G.N.; Cozzarelli, I.M. Processes affecting $\delta^{34}S$ and $\delta^{1}8O$ values of dissolved sulfate in alluvium along the Canadian River, central Oklahoma, USA. *Chem. Geol.* **2009**, *265*, 455–467. [CrossRef]
15. Ingri, J.; Torssander, P.; Andersson, P.S.; Mrth, C.M.; Kusakabe, M. Hydrogeochemistry of sulfur isotopes in the Kalix River catchment, northern Sweden. *Appl. Geochem.* **2015**, *12*, 483–496. [CrossRef]
16. Li, X.Q.; Zhang, B.; Zhou, A.G.; Liu, Y.D. Using sulfur and oxygen isotopes of sulfate to track groundwater contamination from coal mine. *Hydrogrol. Eng. Geol.* **2014**, *41*, 103–109.
17. Stempvoort, D.; Krouse, H.R. Controls of $\delta^{18}O$ in sulphate: Review of experimental data and application to specific environments. *Environ. Geochem. Sulfide Oxid.* **1994**, *31*, 447–479.
18. Ma, K. Water Chemistry and Sulfur-Oxygen Isotopes Geochemistry Characteristics of Xijiang River. Master's Thesis, China University of Geosciences, Beijing, China, 2019.
19. Zhao, C.H.; Liang, Y.P.; Lu, H.P.; Tang, C.L.; Shen, H.Y.; Wang, Z.H. Chemical characteristics and environmental significance of SO_4^{2-} and sulfur isotope in the karst. *Carsologica Sin.* **2019**, *38*, 867–875.
20. Akcil, A.; Koldas, S. Acid mine drainage (AMD): Causes, treatment and case studies. *J. Clean. Prod.* **2005**, *14*, 1139–1145. [CrossRef]
21. Liu, H.T. A Numerical Simulation on the Influence of Underground Water Flow Regime Caused by Coal Mining in Taiyuan Xishan Coal Area. Master's Thesis, Taiyuan University of Technology, Taiyuan, China, 2005.
22. Lu, S.S. Hydrogeochemical Evolution Characteristics and Simulation of Karst Groundwater in the Jinci Spring Area. Master's Thesis, Taiyuan University of Technology, Taiyuan, China, 2021.
23. Bao, H. Purifying barite for oxygen isotope measurement by dissolution and reprecipitation in a chelating solution. *Anal. Chem.* **2006**, *78*, 304–309. [CrossRef]
24. *DZ/T 0064.49-2021*; Methods for Analysis of Groundwater Quality—Part 49: Determination of Carbonated, Bicarbonate Ions, Hydroxy—Titration. Ministry of Natural Resources of China: Beijing, China, 2021.
25. Zhang, H.L.; Wang, C.; Pang, W.; Teng, Y.; Qi, H. Using sulfur and oxygen isotope to trace the source of sulphate in Baotuquan spring area of Jinan. *Geol. Surv. China* **2019**, *6*, 75–80.
26. *GB/T 14848-2017*; Standard for Groundwater Quality. Standardization Administration of China: Beijing, China, 2017.
27. Qureshi, A.; Maurice, C.; Öhlander, B. Potential of coal mine waste rock for generating acid mine drainage. *J. Geochem. Explor.* **2016**, *160*, 44–54. [CrossRef]
28. Liu, M.; Seyf-Laye, A.M.; Ibrahim, T.; Gbandi, D.; Chen, H. Tracking sources of groundwater nitrate contamination using nitrogen and oxygen stable isotopes at Beijing area, China. *Environ. Earth Sci.* **2014**, *72*, 707–715.
29. Chen, D.; Feng, Q.; Liang, H. Effects of long-term discharge of acid mine drainage from abandoned coal mines on soil microorganisms: Microbial community structure, interaction patterns, and metabolic functions. *Environ. Sci. Pollut. Res.* **2021**, *28*, 53936–53952. [CrossRef] [PubMed]
30. Wang, K. Hydrogeochemical Characteristic Analysis and Hydrogeochemical Simulation of Karst Groundwater in Jinci Spring Area. Master's Thesis, Taiyuan University of Technology, Taiyuan, China, 2016.
31. Dou, J.; Du, C.Y.; Qiao, X.J.; Zhou, J.L.; Zhou, P.P.; Li, G.M.; Wu, R.J.; Sun, Z.H. Hydrochemical features of Xishan karst groundwater system in Taiyuan. *Carsologica Sin.* **2008**, *27*, 353–358.
32. Soulsby, C.; Chen, M.; Ferrier, R.C.; Helliwell, R.C.; Jenkins, A.; Harriman, R. Hydrogeochemistry of shallow groundwater in an upland Scottish catchment. *Hydrol. Process.* **2015**, *12*, 1111–1127. [CrossRef]
33. Ren, K.; Zeng, J.; Liang, J.; Yuan, D.; Pan, X. Impacts of acid mine drainage on karst aquifers: Evidence from hydrogeochemistry, stable sulfur and oxygen isotopes. *Sci. Total. Environ.* **2020**, *761*, 143223. [CrossRef]
34. Zhou, X.; Ye, Y.H. Improvement and application of Schukalev groundwater hydrochemical classification method:taking groundwaters in Jinjiang city, Fujian Province as an example. *Resour. Surv. Environ.* **2014**, *35*, 299–304.

35. Jia, X.C.; Zhou, J.W.; Zhu, H.H.; Yu, L.; Zhang, Q.X.; Zhu, Y. Characteristics of sulfur isotope in water bodies near the Zhaoyuan gold mine area and its indicative function of pollution sources. *Hydrogrology Eng. Geol.* **2020**, *47*, 179–188.
36. Okiongbo, K.S.; Akpofure, E. Identification of hydrogeochemical processes in groundwater using major ion chemistry: A case study of Yenagoa and environs, southern Nigeria. *Glob. J. Geol. Sci.* **2015**, *12*, 39–52. [CrossRef]
37. Chidambaram, S.; Anandhan, P.; Prasanna, M.V.; Srinivasamoorthy, K.; Vasanthavigar, M. Major ion chemistry and identification of hydrogeochemical processes controlling groundwater in and around Neyveli Lignite Mines, Tamil Nadu, South India. *Arab. J. Geosci.* **2013**, *6*, 3451–3467. [CrossRef]
38. Ren, K.; Pan, X.D.; Lan, G.J.; Peng, C.; Liang, J.P.; Zeng, J. Seasonal variation and sources identification of dissolved sulfate in a typical karst subterranean stream basin using sulfur and oxygen isotope. *Environ. Sci.* **2021**, *42*, 4267–4274.
39. Zhang, Q.; Wang, H.; Lu, C. Tracing sulfate origin and transformation in an area with multiple sources of pollution in northern China by using environmental isotopes and Bayesian isotope mixing model. *Environ. Pollut.* **2020**, *265*, 115105. [CrossRef] [PubMed]
40. Wang, Y.J.; Hu, Y.Y.; Ren, J.F.; Qu, K.; Yin, N.; Yu, H.J.; Ma, G.G. Sulfur and lead isotope composition and tracing for sources of ore-forming materials in Beiming river iron deposits, southern Taihang mountains. *Geoscience* **2011**, *25*, 846–852.
41. Tang, C.L.; Zheng, X.Q.; Liang, Y.P. Hydrochemical characteristics and formation causes of ground karst water systems in the Longzici spring catchment. *Environ. Sci.* **2020**, *41*, 2087–2095.
42. Xiao, H.Y.; Liu, C.Q.; Li, S.L. Geochemical characteristics of sulfur and nitrogen isotopic compositions in rains of Guiyang in summer. *Geochimica* **2003**, *32*, 248–254.
43. Zhang, D.; Yang, J.M.; Huang, X.Y.; Liu, S.T.; Zhang, Z.Y. Sources of dissolved heavy metals in river water of the Yiluo River basin based on sulfur isotope of sulfate. *China Environ. Sci.* **2019**, *39*, 2549–2559.
44. Petelet-Giraud, E.; Klaver, G.; Negrel, P. Natural versus anthropogenic sources in the surface- and groundwater dissolved load of the Dommel river (Meuse basin): Constraints by boron and strontium isotopes and gadolinium anomaly. *J. Hydrol.* **2009**, *369*, 336–349. [CrossRef]
45. Pan, S.L. Application of stable isotope to the research on karst water in Taiyuan area. *Carsologica Sin.* **1989**, *8*, 151–155.
46. Tang, C.L.; Zheng, X.Q.; Liang, Y.P.; Zhang, F.W.; Jing, Z. The hydraulic connection between Jinci and Pingquan in Taiyuan Shanxi and its contribution to the reflow of Jinci spring. *Geol. China* **2020**, *47*, 1755–1764.